Yang, He; Khayrudinov, Vladislav; Dhaka, Veer; Jiang, Hua; Autere, Anton; Jussila, Henri; Lipsanen, Harri; Sun, Zhipei

Nanowire network–based multifunctional all-optical logic gates

Published in:
Science Advances

DOI:
10.1126/sciadv.aar7954

Published: 27/07/2018

Document Version
Publisher's PDF, also known as Version of record

APPLIED SCIENCES AND ENGINEERING

Nanowire network–based multifunctional all-optical logic gates

He Yang[1], Vladislav Khayrudinov[1], Veer Dhaka[1], Hua Jiang[2], Anton Autere[1], Harri Lipsanen[1], Zhipei Sun[1,3]*, Henri Jussila[1]*

All-optical nanoscale logic components are highly desired for various applications because light may enable logic functions to be performed extremely quickly without the generation of heat and cross-talk. All-optical computing at nanoscale is therefore a promising alternative but requires the development of a complete toolbox capable of various logic functionalities. We demonstrate nanoscale all-optical switches by exploiting the polarization-dependent light emission property of crossbar InP and AlGaAs nanowire networks. These networks can perform various logic operations, such as AND, OR, NAND, and NOR binary logic functions. Furthermore, on the basis of these logic operations, our networks successfully enable all-optical arithmetic binary calculations, such as *n*-bit addition, to be conducted. Our results underscore the promise of assembled semiconductor nanowire networks as a building block of on-chip all-optical logic components for future nanophotonics.

INTRODUCTION

Current limitations of modern integrated circuits, resulting from the prolonged scaling of the transistors, are propelling intense activities in the field of nanophotonics (*1*, *2*). In this respect, integration of all-optical nanoprocessors into future integrated circuits may drive the computers to perform their functions ever more effectively compared to their modern electronic counterparts (*3*). For this purpose, it is important to realize a complete toolbox filled with chip-integrable all-optical nanoscale components (for example, light sources, switches, waveguides, modulators, and logic gates). Over the last few decades, the main research trends in this area have focused toward the development of all-optical logic devices based on nonlinear optical effects in silicon waveguide circuits (*4*–*6*) and semiconductor optical amplifiers (*7*, *8*). More recently, nanowires (NWs) have emerged as promising alternative candidates to fulfill the toolbox. From the basic science perspective, these NW structures are fascinating since they provide new means to construct all-optical logic components owing to their extraordinary properties including strong waveguiding effects (*9*–*11*), optical nonlinearity (*12*, *13*), and plasmonic effects (*14*, *15*) combined with their subwavelength diameter. Because of these properties in particular, various NW-based components have been demonstrated in the field of nanophotonics, such as electrically driven lasers (*16*), electro-optical modulators (*17*), and also, as noted, all-optical logic gates (*11*, *14*, *15*). Among those components, logic gates form the core of the data processing and are therefore of particular importance in the construction of all-optical nanoprocessor circuits.

The NW-based all-optical logic gates have thus far exploited the stimulated scattering of exciton-polaritons in CdS NWs (*11*) and plasmonic interference effects in Ag NW networks (*14*, *15*). As such, the realization of the conditions suitable for all-optical switching requires complex fabrication steps and delicate measurement schemes. For instance, since the switching in the CdS NW-based device is dependent on the pump-excited polaritons inside the NWs, the operation occurs only at low temperature (inside a liquid nitrogen–cooled cryostat) and requires a gallium ion milling fabrication step to obtain efficient light coupling within the NW waveguides (*11*). On the other hand, Ag NW-based logic gates demand interference conditions obtained by accurately positioning each individual NW with a micromanipulator setup. Hence, the practicality of these approaches is largely limited by the fabrication process, and therefore, it is of great importance to demonstrate new approaches better suited for the realization of future all-optical nanoprocessor circuits capable of complex logic operations. In this study, to achieve this target, we use a scalable fabrication process without any lithography steps to prepare crossbar networks of InP and AlGaAs NWs. The fabricated semiconductor NW network operates as a polarization-controlled all-optical wavelength switch. The polarization-controlled operation mode of the switch is based on the anisotropic structure of the NWs, which makes their emission extremely sensitive to the excitation light polarization direction (*18*). Thus, the linear optics explained the operation principle of our switch well, in contrast to all previously reported NW-based all-optical logic gates (*11*, *14*, *15*). Furthermore, InP and AlGaAs NWs are selected because their bandgap energy differs considerably, making the all-optical wavelength switching very easily resolvable (wavelength shift as large as more than ~200 nm, that is, from ~665 to ~890 nm). Compared to GaAs NWs, our InP and AlGaAs NWs are also found to show photoluminescence (PL) emission at room temperature due to the reduced nonradiative surface recombination channels in InP (*19*) and in situ doping of AlGaAs. Our crossbar NW structure allows multiple parallel all-optical logic functions (for example, AND, OR, NAND, and NOR) to be realized. In particular, we perform various binary arithmetic calculations all-optically (such as *n*-bit addition) with these logic gates.

RESULTS AND DISCUSSION

InP and AlGaAs NWs are grown on silicon substrates by using a Au nanoparticle–assisted vapor-liquid-solid (VLS) growth method inside a horizontal-flow metalorganic vapor phase epitaxy (MOVPE) reactor (see the Supplementary Materials for detailed information). The fabrication of (opto)electronic devices from VLS-grown NWs

[1]Department of Electronics and Nanoengineering, Aalto University, Espoo FI-00076, Finland. [2]Department of Applied Physics and Nanomicroscopy Center, Aalto University, Espoo FI-00076, Finland. [3]QTF Centre of Excellence, Department of Applied Physics, Aalto University, FI-00076 Aalto, Finland.
*Corresponding author. Email: henri.jussila@aalto.fi (H.J.); zhipei.sun@aalto.fi (Z.S.)

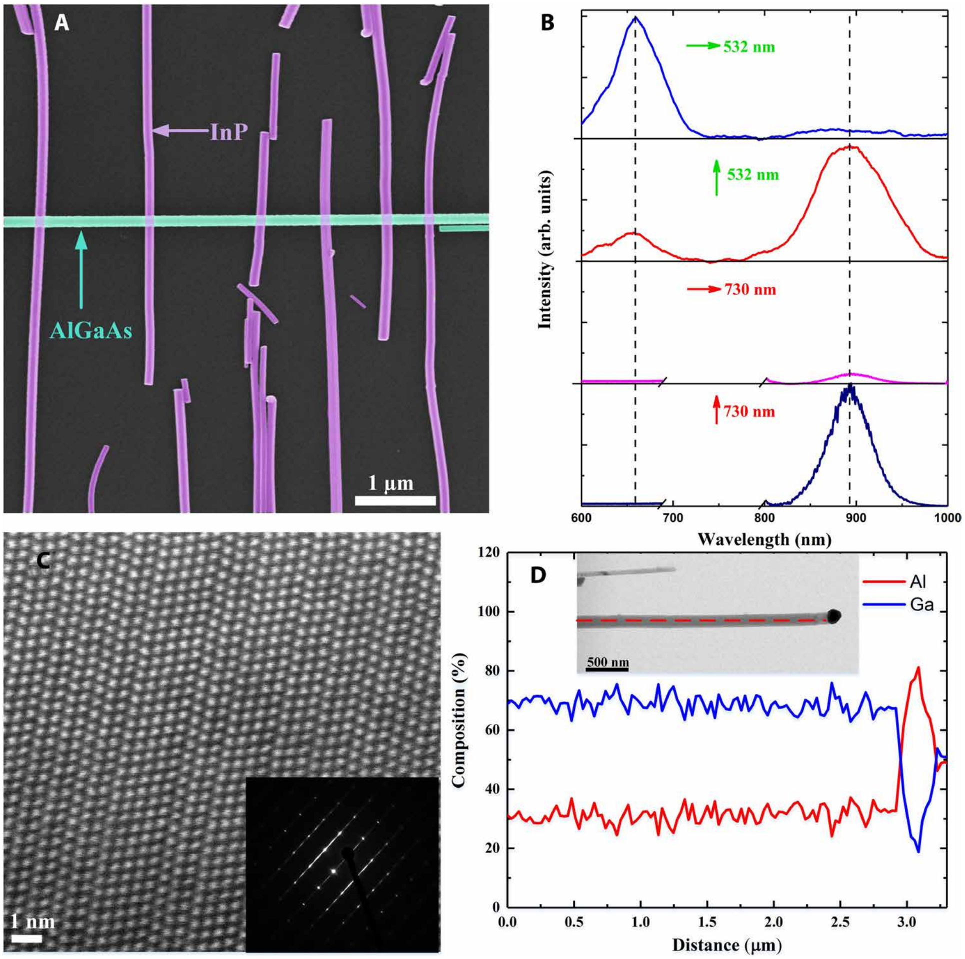

Fig. 1. Structural and optical properties of InP and AlGaAs crossbar NW networks. (**A**) False-color scanning electron microscopy image of the crossbar InP and AlGaAs NW networks (illustrated with different colors); InP NWs are combed along the vertical direction and an AlGaAs NW along the horizontal direction to form six pairs of crossbar junctions. (**B**) PL spectra of the NWs measured at a single exemplary measurement spot. The polarization direction of the excitation lasers (at 532 and 730 nm) is labeled. arb. units, arbitrary units. (**C**) HRSTEM image of InP NWs. The inset shows the diffraction pattern demonstrating the ZB crystal structure and the formation of frequent twin planes along the NW growth axis. (**D**) EDX measurement results of AlGaAas NWs show the Al and Ga composition along the NW growth direction (that is, [111] crystal direction). The line scan location is shown in the inset (*28*).

typically involves complex processing steps [such as focused ion beam milling (*11*), micromanipulation (*14*), electron beam lithography (*20*), etc.] due to unorganized location and tilting of the NWs. To address this constraint, we use a scalable nanocombing method to align the randomly pointing NWs in the horizontal plane, which does not need the abovementioned complex fabrication steps (*21*, *22*). In this way, the as-grown NWs are transferred onto a glass substrate using the nanocombing technique (see fig. S1). It should be noted that this nanocombing step is performed in this work without any micromanipulator setup, illustrating the simplicity of our approach. We estimate that ~95% of NWs are aligned along the same direction within an alignment error of ±10° after the single combing step (see fig. S2). Furthermore, with this method, it is easy to realize crossbar NW junctions by simply combing InP NWs along one direction and the other (that is, AlGaAs) NWs along the perpendicular direction for the fabrication of multifunctional logic gates. Note that, after combing the InP NWs, we deposit a 100-nm-thick SiO_2 layer to isolate the InP NWs from the AlGaAs NWs. Because of the random nature of the process, it is difficult to make every InP NW perpendicular to AlGaAs NW and simultaneously be overlapping; however, it is easy to find many crossbar NW junctions on the target substrate, as shown in Fig. 1A. In such a ~6 μm × 6 μm area, we find six pairs of well-aligned InP and AlGaAs crossbar NW junctions. It verifies that this easy nanocombing method is effective and helpful for the realization of large-area crossbar NW networks.

Polarization-dependent PL measurements are performed on crossbar NW junctions. Figure 1B shows the room temperature PL spectra of an exemplary NW junction measured from a single measurement spot by using the excitation wavelength of 532 or 730 nm with varying excitation laser polarization directions (see details in the Supplementary Materials). Under the 532-nm laser excitation, two PL peaks located at 665 and 890 nm are observed, which we attribute to AlGaAs and InP NWs, respectively. Under the 730-nm laser excitation, only a single PL peak is observed at the wavelength of 890 nm. Note that, in this case, no PL is created at the wavelength of 665 nm because the band-to-band transition energy of AlGaAs NWs is larger than the photon energy of the excitation laser. PL quantum efficiency (PLQE) of the NWs is an important measure to

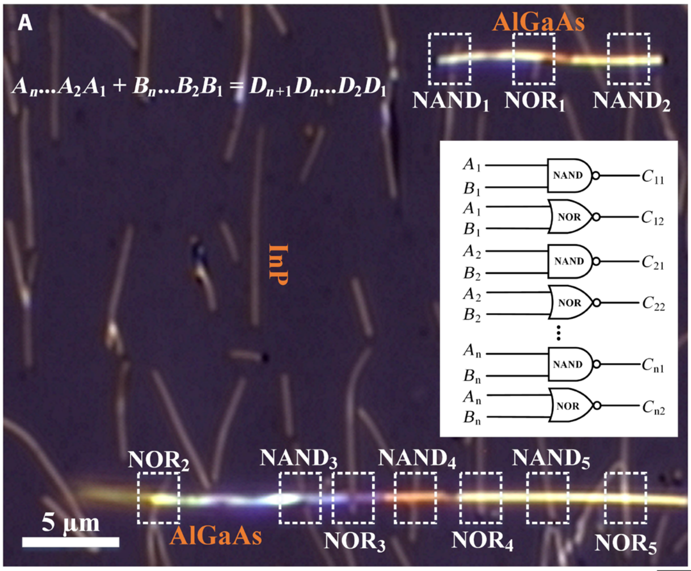

B

NAND			NOR		
Input		Output	Input		Output
A_i (λ)	B_i (polarization)	C_{i1} (PL_{AlGaAs} + PL_{InP})	A_i (λ)	B_i (polarization)	C_{i2} (PL_{AlGaAs})
1 (730 nm)	1 (H)	0	1 (730 nm)	1 (V)	0
1 (730 nm)	0 (V)	1	1 (730 nm)	0 (H)	0
0 (532 nm)	1 (H)	1	0 (532 nm)	1 (V)	0
0 (532 nm)	0 (V)	1	0 (532 nm)	0 (H)	1

C

1st bit				*n*th bit				
C_{11}	C_{12}	D_1	$Carry_1$	C_{n1}	C_{n2}	$Carry_{n-1}$	D_n	$Carry_n$
1	1	0	0	1	1	0	0	0
1	0	1	0	1	1	1	1	0
0	0	0	1	1	0	0	1	0
				1	0	1	0	1
				0	0	0	0	1
				0	0	1	1	1

$$\begin{array}{r} 11010_2 \\ +\ 01110_2 \\ \hline 101000_2 \end{array}$$

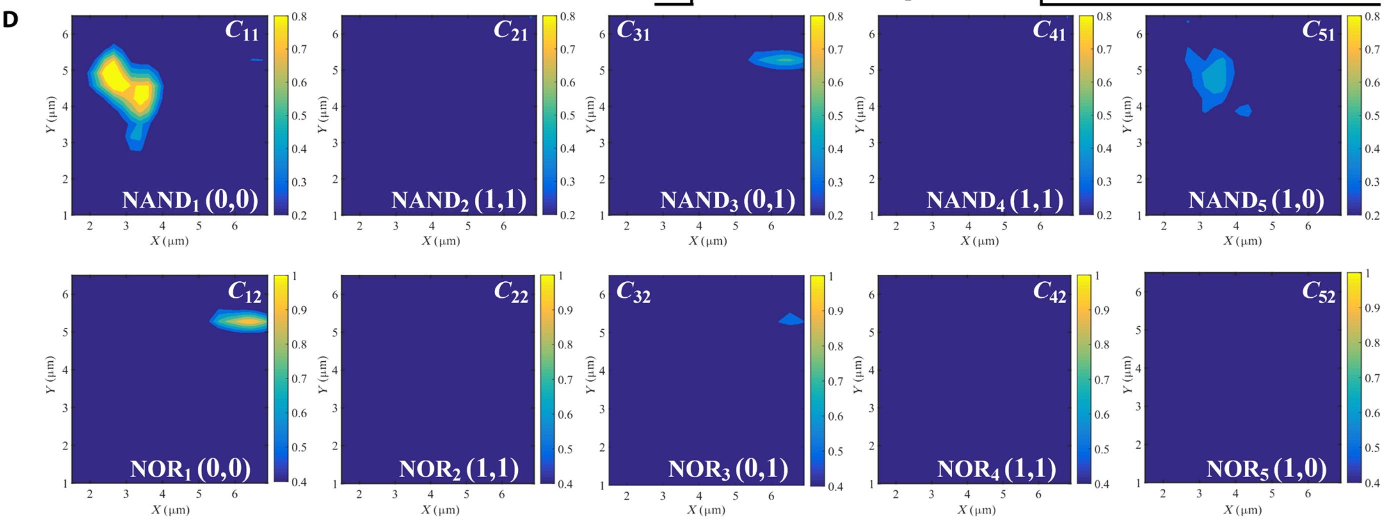

Fig. 2. NW-based all-optical *n*-bit full adder. (**A**) The optical image showing that, after a single combing, 10 AlGaAs and InP crossbar NW junctions exist in 30 µm × 30 µm area. The dashed white boxes highlight the locations where 10 parallel NAND and NOR logic gates can be constructed. (**B**) The truth tables of NOR and NAND logic gates using the polarization-dependent PL property of NWs. (**C**) The rules for obtaining the addition operation result from NAND and NOR logic gate outputs. (**D**) An example showing PL mapping of a single NW junction when the addition operation is performed [that is, 24 (11010_2) is added to 16 (01110_2)]. The addition operation result is obtained by following the rules shown in (C) (*28*).

consider for the assessment of optical properties of our crossbar NW structures. So far, the external QEs of NWs have typically been reported with a range of 10^{-5} to 10^{-2} (*23*). In this work, by comparing the PL intensity of our NWs to that of Rhodamine 6G, we estimate the PLQE of our NWs to be ~10^{-4}, still sufficient for the results presented later in this work.

To verify the observed PL transitions, a structural analysis is performed by high-resolution scanning transmission electron microscopy (HRSTEM) and energy-dispersive x-ray (EDX) measurements (see the Supplementary Materials for details). As shown in Fig. 1C, the structure of InP NWs is predominantly zinc-blende (ZB) with frequent twin planes along the whole NW length (rotationally twinned ZB InP NWs). Compared to the room temperature PL peak of bulk ZB InP at the wavelength of ~920 nm, the ~30-nm blue shift in the PL peak position of the InP NWs can be attributed to these frequent twin faults (*24*–*27*). On the other hand, PL properties of AlGaAs NWs depend strongly on the elemental compositions and the crystal quality. As shown in fig. S3, the crystal structure of AlGaAs NWs is predominantly ZB with a small concentration of crystal defects. Figure 1D shows a typical EDX line scan of AlGaAs NWs along the [111] crystal direction, revealing an initial Al composition of 80% within a very short region of the NW tip. The high Al composition in the vicinity of Au catalyst is attributed to the incorporation of extra Al left in the Au droplet to the NW body during the cooling period. Thereafter, an Al composition of ~30% (±5%) is measured from various NWs along the whole NW body. The calculated bandgap energy for AlGaAs with the Al composition within the error margins corresponds to the emission wavelengths ranging from 665 to 714 nm and is overall in the same range as the observed PL peaks. Hence, the above structural characterization agrees with the PL measurement results.

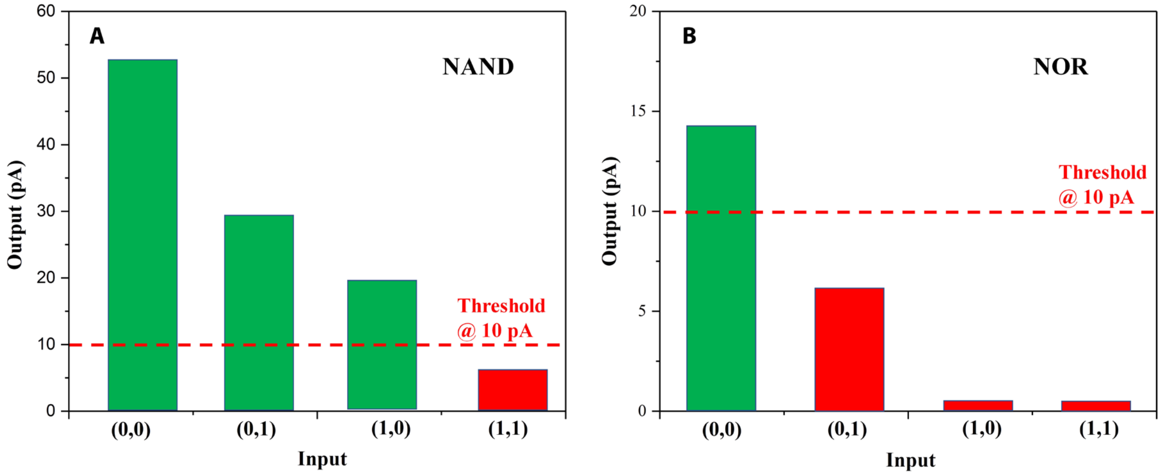

Fig. 3. System-level demonstrated all-optical logic gate outputs. All-optical logic gate outputs of our proof-of-principle system-level demonstration under different input configurations for NAND (**A**) and NOR (**B**) logic operations.

As shown in Fig. 1B, the relative magnitude of the PL peaks depends strongly on the polarization direction of the excitation laser due to the one-dimensional structural confinement of NWs (*18*). When the polarization direction of the 532-nm excitation laser is parallel to the AlGaAs alignment axis (that is, horizontal; Fig. 1A), the PL signal emerges at the wavelength of 665 nm. In contrast, when the laser polarization direction is aligned along the InP alignment axis (that is, vertical; Fig. 1A), the PL signal is observed at the wavelength of 890 nm (*28*). On the other hand, when the laser at the 730-nm wavelength is used, the PL peak appears strongly with the laser polarization direction parallel to the InP alignment axis, while the PL peak nearly disappears at the corresponding vertical direction. The degrees of polarization (DOP) of 94 and 65% are obtained for InP and AlGaAs PL peak intensities, respectively, as shown in fig. S4. The slightly smaller DOP in the case of AlGaAs is attributed to the larger AlGaAs NW diameter than that of InP NWs (as described in the Supplementary Materials), therefore making these AlGaAs NWs less sensitive to the excitation laser polarization direction. Nevertheless, the crossbar NW junction allows the polarization direction of the laser to select whether InP or AlGaAs NW emits PL. Since their PL wavelengths (that is, 665 nm for AlGaAs NWs and 890 nm for InP NWs) are different, our crossbar NW junction is capable of operating as polarization-controlled all-optical wavelength switch (under 532-nm laser excitation) and polarization-controlled all-optical intensity switch (under 730-nm laser excitation). The dimensions of our structure are in subwavelength scale (NW diameter smaller than 120 nm), thereby suggesting that our crossbar NW junctions could be used in future on-chip nanophotonic networks. Further, we note that the observed switching effect originates from the linear optics, in contrast to previously reported all-optical NW-based switches (*11*, *14*).

Using the polarization-dependent PL wavelength switch, we construct all-optical nanoscale NAND and NOR logic gates (depicted in Fig. 2A). Figure 2B shows the truth tables of our proposed all-optical NAND and NOR logic gates. For the NAND function, the excitation laser wavelength and the polarization direction mark the logic gate input state (A_i, B_i), respectively, while the PL signal from the NW junctions returns the logic gate output (that is, C_{ij}, with $j = 1$ implying the NAND function in the following discussion). The NAND function can be realized by defining the PL signal at the wavelength range covering only the bandgaps of AlGaAs and InP NWs as the NAND logic gate output [that is, $\lambda_{PL} \in$ (620 nm, 690 nm) $\wedge$ (860 nm, 940 nm)]. As a result, if the PL signal appears in this wavelength range, the NAND gate returns an output of 1. In addition, an output of 0 (that is, a very weak PL signal) is only obtained if the NAND gate is excited by the 730-nm laser (corresponding to the input state of $A_i = 1$) with the polarization direction along the AlGaAs alignment axis (corresponding to the input state of $B_i = 1$). For the NOR function, on the other hand, the gate input is coded similarly in the excitation laser wavelength (A_i) and the corresponding laser's polarization direction (B_i), with the difference that the polarization direction in the gate input B_i is opposite to that of the NAND function. As illustrated in Fig. 2B, the PL signal at wavelength range, covering only the AlGaAs NWs, defines the NOR gate output (that is, C_{ij}, with $j = 2$ for the NOR function). As a result, the gate output of 1 is obtained if the PL signal emerges in this wavelength range [that is, $\lambda_{PL} \in$ (620 nm, 690 nm)]. Otherwise, the NOR gate returns an output of 0. Based on this definition, only the 532-nm laser excitation wavelength and the polarization direction along the alignment axis of AlGaAs NWs (corresponding to the input state of $A_i = 0$ and $B_i = 0$) allows the NOR gate to return an output of 1 (*28*). Moreover, it is noteworthy to mention that, by defining our NW-based logic gate output similarly but the input differently, the NW junction can also be used for the construction of OR and AND logic functions (see fig. S5). Hence, this further highlights the multifunctional performance of our NW-based all-optical logic gates.

Our aligned NW structure allows light to perform arithmetic functions, such as addition operation. The result of an addition operation of any two bits (that is, $A = A_n \ldots A_2A_1$ and $B = B_n \ldots B_2B_1$) can be obtained from the outputs of n pairs of parallel NAND and NOR logic gates. To simplify the situation, we first describe how our all-optical NAND and NOR logic gates enable the result of 1-bit addition operation to be unambiguously achieved. In case 0_2 is added to 0_2 (with subscript 2 defining the number as a binary number), the inputs of NAND and NOR gates (that is, $A_1 = 0$ and $B_1 = 0$) will result in gate outputs of $C_{11} = 1$ and $C_{12} = 1$, respectively. On the other hand, if 0_2 is added to 1_2 (or 1_2 to 0_2), the gate inputs of $A_1 = 0$ (or 1) and $B_1 = 1$ (or 0) will produce gate outputs of $C_{11} = 1$ and $C_{12} = 0$. Furthermore, the NAND and NOR logic gates will only return outputs of $C_{11} = 0$ and $C_{12} = 0$ when both gate inputs are 1 (that is, $A_1 = 1$ and $B_1 = 1$). Therefore, the result (that is, $D = D_2D_1$) of the two 1-bit addition operations can be unambiguously obtained from the gate outputs since three different gate output configurations are possible. By following the same order as above, the gate output configurations are defined to return a result of $D = 00_2$, $D = 01_2$, and $D = 10_2$, as shown in Fig. 2C, which is consistent with the binary addition operation result (*28*). Note that a more complex situation is an addition operation of two n-bit numbers (A and B as above), since the possibility of carry information needs to be considered. Nevertheless, the carry information can be accounted for, and the result of the addition operation can still be obtained from the outputs of n pairs of NAND and NOR logic gates by following the rules shown in Fig. 2C.

Figure 2D shows an example of the logic gate outputs, when a single crossbar NW junction performs an addition operation of two 5-bit numbers ($11010_2 + 01110_2$). In this calculation, the operation of a single NAND and NOR gate is also presented under all four different input conditions (A_i, B_i). As shown in PL maps of the NAND gate, the PL signal (threshold value for PL ~ 0.3) emerges with the (0,0), (1,0), and (0,1) gate inputs, while no PL signal arises under (1,1) input state, in agreement with our proposed all-optical NAND function described above. The operation of the NOR gate is proven similarly. As shown in Fig. 2D, the PL signal (threshold value for PL ~ 0.6) is generated only when the NOR gate input state is (0,0). Since all the other gate input states return an output of 0, the realization of the NOR function is experimentally verified. The result of the exemplary addition operation can also be resolved by following the rules shown in Fig. 2C, with the final carry information placed as the largest bit (*28*). Applying the rules of Fig. 2C to PL maps, the correct number of 101000_2 is obtained for the $11010_2 + 01110_2$ binary number addition operation.

In addition to a high-sensitivity commercial micro-PL (μ-PL) system used in the previous demonstration, we build an optical system that reads the gate output with a silicon photodiode to prove that our all-optical NW-based logic gates can be realized at a system level. Figure S6 shows the schematics of the proof-of-principle system-level demonstration. The logic gate input is coded, as above, into the excitation wavelength and the polarization direction, and a silicon photodiode measures the gate output. Figure 3 shows the results. As shown in Fig. 3, both the NOR and NAND gates return an output of 1 when the photodiode gives a signal larger than 10 pA (threshold limit), in agreement with the truth tables shown in Fig. 2B.

It should be noted that n-bit subtraction and 2-bit multiplication operations can also be performed with our multifunctional all-optical NW logic gates. Subtraction operation, for instance, requires only the largest bit of the n-bit addition operation to define the sign of the number (that is, $A = -2^{n-1}A_n + 2^{n-2}A_{n-1} + \ldots + 2A_2 + A_1$), while the 2-bit multiplication operations can be performed with the NW-based all-optical logic circuit as shown in fig. S7. As the multifunctionality of these NW structures combined to scalable fabrication process suggests, these nanostructures are interesting alternative candidates to be used in future all-optical nanoprocessors.

CONCLUSIONS

In summary, we demonstrate a method to construct a nanoscale all-optical wavelength switch based on the polarization-dependent PL properties of the crossbar InP and AlGaAs NW networks. The structure is formed without any lithography process by combing InP and AlGaAs NWs along the two perpendicular directions, allowing the emission wavelength of the crossbar structure to be tuned over 200 nm by altering the excitation laser polarization direction. This polarization-controlled behavior allows the fabrication of multiple parallel all-optical logic gates with subwavelength dimension. By using the fabricated multifunctional all-optical logic gates with AND, OR, NAND, and NOR functions, our structure successfully enables the light to perform the binary arithmetic operations such as n-bit addition. Overall, our results underscore that such a NW network is an interesting candidate for future all-optical nanophotonic devices. In particular, the reported NW building block provides a scalable alternative to be used in future all-optical nanoprocessor circuits. These conclusions were also drafted in the doctoral dissertation of the first author (*28*).

MATERIALS AND METHODS

NW growth

InP and AlGaAs NWs were fabricated on Si (111) substrates inside a horizontal-flow atmospheric pressure MOVPE system. Trimethylaluminum (TMAl), trimethylgallium (TMGa), tertiarybutylarsine (TBA), trimethylindium (TMIn), and tertiarybutylphosphine (TBP) were used as precursors for AlGaAs and InP NWs. Diethylzinc (DEZn) was used for the doping of AlGaAs NWs to enhance their PL properties. Before growth, 40- and 60-nm-diameter gold (Au) nanoparticles from a colloidal solution (BBI International) were dropcasted as catalysts for the VLS growth of InP and AlGaAs NWs, respectively.

NW combing

After synthesis, the as-grown NWs were transferred onto a glass substrate by using a nanocombing method (that is, mechanically sliding the NW substrate over the target substrate along one direction). This technique allows the randomly directed NWs on silicon substrate to self-align in the horizontal plane and point toward one direction. Thus, the crossbar NW structures of InP and AlGaAs NWs examined in this work were fabricated by combing InP NWs along one direction and AlGaAs NWs along the perpendicular direction. Note that, after combing the NWs of the first material, a 100-nm-thick plasma-enhanced chemical vapor deposition (PECVD) SiO_2 layer was deposited (PECVD 80+,Oxford Instruments) to isolate InP NWs from AlGaAs NWs.

TEM characterization

HRSTEM measurements were carried out with a JEOL 2200FS double aberration–corrected field emission gun microscope operated at 200 kV. Elemental composition in the AlGaAs NW body was determined using a TEM-integrated EDX spectroscopy tool. To prepare a sample for TEM study, a 400-mesh copper grid (3 mm in diameter) covered with a holey supporting film was used to slightly scratch the surface of the Si substrate with as-grown NWs, allowing individual NWs to be found for structural analysis.

PL measurement

All μ-PL measurements performed in this work were carried out at room temperature with WITec alpha300S scanning near-field optical microscopy under confocal operation mode. In these measurements, linearly polarized 532- and 730-nm laser sources were used for excitation. Polarization-dependent PL measurements were performed by rotating the incident light polarization direction with a half waveplate. The polarization angle was defined as the angle between the horizontal direction (in all the shown images) and the direction toward which the electric field of the linearly polarized excitation laser was pointing. The PLQE numbers reported in this work were evaluated by comparing the PL intensity of NWs to that measured from the known reference sample (that is, Rhodamine 6G).

SUPPLEMENTARY MATERIALS

Supplementary material for this article is available at http://advances.sciencemag.org/cgi/content/full/4/7/eaar7954/DC1
Section S1. NW growth
Section S2. NW combing
Section S3. TEM characterization
Section S4. PL measurements
Section S5. NW-based all-optical AND and OR gates
Section S6. System-level demonstration of logic gate operations
Section S7. NW-based multiplication operation
Fig. S1. SEM characterization of NWs.
Fig. S2. NW combing statistics.
Fig. S3. TEM characterization of AlGaAs NWs.
Fig. S4. Polarization dependent PL properties of NWs.
Fig. S5. Truth tables of AND and OR logic gates using the polarization-dependent PL properties of crossbar NW networks.
Fig. S6. Schematics of our system-level demonstration of the logic gates.
Fig. S7. NW-based all-optical 2-bit multiplier.

REFERENCES AND NOTES

1. R. Kirchain, L. C. Kimerling, A roadmap for nanophotonics. *Nat. Photonics* **1**, 303–305 (2007).
2. N. Engheta, Circuits with light at nanoscales: Optical nanocircuits inspired by metamaterials. *Science* **317**, 1698–1702 (2007).
3. H. J. Caulfield, S. Dolev, Why future supercomputing requires optics. *Nat. Photonics* **4**, 261–263 (2010).
4. V. R. Almeida, C. A. Barrios, R. R. Panepucci, M. Lipson, All-optical control of light on a silicon chip. *Nature* **431**, 1081–1084 (2004).
5. Q. Xu, M. Lipson, All-optical logic based on silicon micro-ring resonators. *Opt. Express* **15**, 924–929 (2007).
6. M. Xiong, L. Lei, Y. Ding, B. Huang, H. Ou, C. Peucheret, X. Zhang, All-optical 10 Gb/s AND logic gate in a silicon microring resonator. *Opt. Express* **21**, 25772–25779 (2013).
7. G. Berrettini, A. Simi, A. Malacarne, A. Bogoni, L. Poti, Ultrafast integrable and reconfigurable XNOR, AND, NOR, and NOT photonic logic gate. *IEEE Photonics Technol. Lett.* **18**, 917–919 (2006).
8. Z. Li, G. Li, Ultrahigh-speed reconfigurable logic gates based on four-wave mixing in a semiconductor optical amplifier. *IEEE Photonics Technol. Lett.* **18**, 1341–1343 (2006).
9. H.-G. Park, C. J. Barrelet, Y. Wu, B. Tian, F. Qian, C. M. Lieber, A wavelength-selective photonic-crystal waveguide coupled to a nanowire light source. *Nat. Photonics* **2**, 622–626 (2008).
10. L. K. van Vugt, B. Zhang, B. Piccione, A. A. Spector, R. Agarwal, Size-dependent waveguide dispersion in nanowire optical cavities: Slowed light and dispersionless guiding. *Nano Lett.* **9**, 1684–1688 (2009).
11. B. Piccione, C.-H. Cho, L. K. van Vugt, R. Agarwal, All-optical active switching in individual semiconductor nanowires. *Nat. Nanotechnol.* **7**, 640–645 (2012).
12. C. F. Zhang, Z. W. Dong, G. J. You, R. Y. Zhu, S. X. Qian, H. Deng, H. Cheng, J. C. Wang, Femtosecond pulse excited two-photon photoluminescence and second harmonic generation in ZnO nanowires. *Appl. Phys. Lett.* **89**, 042117 (2006).
13. J. P. Long, B. S. Simpkins, D. J. Rowenhorst, P. E. Pehrsson, Far-field imaging of optical second-harmonic generation in single GaN nanowires. *Nano Lett.* **7**, 831–836 (2007).
14. H. Wei, Z. Wang, X. Tian, M. Käll, H. Xu, Cascaded logic gates in nanophotonic plasmon networks. *Nat. Commun.* **2**, 387 (2011).
15. H. Wei, Z. Li, X. Tian, Z. Wang, F. Cong, N. Liu, S. Zhang, P. Nordlander, N. J. Halas, H. Xu, Quantum dot-based local field imaging reveals plasmon-based interferometric logic in silver nanowire networks. *Nano Lett.* **11**, 471–475 (2010).
16. X. Duan, Y. Huang, R. Agarwal, C. M. Lieber, Single-nanowire electrically driven lasers. *Nature* **421**, 241–245 (2003).
17. A. B. Greytak, C. J. Barrelet, Y. Li, C. M. Lieber, Semiconductor nanowire laser and nanowire waveguide electro-optic modulators. *Appl. Phys. Lett.* **87**, 151103 (2005).
18. J. Wang, M. S. Gudiksen, X. Duan, Y. Cui, C. M. Lieber, Highly polarized photoluminescence and photodetection from single indium phosphide nanowires. *Science* **293**, 1455–1457 (2001).
19. H. J. Joyce, C. J. Docherty, Q. Gao, H. H. Tan, C. Jagadish, J. Lloyd-Hughes, L. M. Herz, M. B. Johnston, Electronic properties of GaAs, InAs and InP nanowires studied by terahertz spectroscopy. *Nanotechnology* **24**, 214006 (2013).
20. Y. Huang, X. Duan, Y. Cui, L. J. Lauhon, K.-H. Kim, C. M. Lieber, Logic gates and computation from assembled nanowire building blocks. *Science* **294**, 1313–1317 (2001).
21. Y. Huang, X. Duan, Q. Wei, C. M. Lieber, Directed assembly of one-dimensional nanostructures into functional networks. *Science* **291**, 630–633 (2001).
22. J. Yao, H. Yan, C. M. Lieber, A nanoscale combing technique for the large-scale assembly of highly aligned nanowires. *Nat. Nanotechnol.* **8**, 329–335 (2013).
23. T. Burgess, D. Saxena, S. Mokkapati, Z. Li, C. R. Hall, J. A. Davis, Y. Wang, L. M. Smith, L. Fu, P. Caroff, H. H. Tan, C. Jagadish, Doping-enhanced radiative efficiency enables lasing in unpassivated GaAs nanowires. *Nat. Commun.* **7**, 11927 (2016).
24. A. Mishra, L. V. Titova, T. B. Hoang, H. E. Jackson, L. M. Smith, J. M. Yarrison-Rice, Y. Kim, H. J. Joyce, Q. Gao, H. H. Tan, C. Jagadish, Polarization and temperature dependence of photoluminescence from zincblende and wurtzite InP nanowires. *Appl. Phys. Lett.* **91**, 263104 (2007).
25. J. Bao, D. C. Bell, F. Capasso, J. B. Wagner, T. Mårtensson, J. Trägårdh, L. Samuelson, Optical properties of rotationally twinned InP nanowire heterostructures. *Nano Lett.* **8**, 836–841 (2008).
26. Z. Ikonić, G. P. Srivastava, J. C. Inkson, Electronic properties of twin boundaries and twinning superlattices in diamond-type and zinc-blende-type semiconductors. *Phys. Rev. B* **48**, 17181–17193 (1993).
27. L. Gao, R. L. Woo, B. Liang, M. Pozuelo, S. Prikhodko, M. Jackson, N. Goel, M. K. Hudait, D. L. Huffaker, M. S. Goorsky, S. Kodambaka, R. F. Hicks, Self-catalyzed epitaxial growth of vertical indium phosphide nanowires on silicon. *Nano Lett.* **9**, 2223–2228 (2009).
28. H. Yang, thesis, Aalto University (2018).

Acknowledgments
Funding: We acknowledge funding from Academy of Finland (grants nos. 284529, 276376, 284548, 295777, 298297, 312551, 312297, 314810, and 304666), TEKES (NP-Nano, OPEC), the Micronova Nanofabrication Centre of Aalto University, the European Union's Seventh Framework Programme (grant no. 631610), China Scholarship Council and Nokia Foundation, the Walter Ahlström Foundation, and Aalto University Doctoral School. **Author contributions:** H.Y. and H. Jussila designed and performed the experiments, wrote the manuscript, and conceived the work. V.K. and V.D. fabricated the NW samples using the MOVPE method. H. Jiang did the TEM experiments. A.A., H.L., and Z.S. participated in the analysis of data. All authors discussed the results, commented on the manuscript, and gave approval for the final version of the manuscript. **Competing interests:** The authors declare that they have no competing interests. **Data and materials availability:** All data needed to evaluate the conclusions in the paper are present in the paper and/or the Supplementary Materials. Additional data related to this paper may be requested from the authors.

Submitted 18 December 2017
Accepted 13 June 2018
Published 27 July 2018
10.1126/sciadv.aar7954

Citation: H. Yang, V. Khayrudinov, V. Dhaka, H. Jiang, A. Autere, H. Lipsanen, Z. Sun, H. Jussila, Nanowire network–based multifunctional all-optical logic gates. *Sci. Adv.* **4**, eaar7954 (2018).

Nanowire network–based multifunctional all-optical logic gates

He Yang, Vladislav Khayrudinov, Veer Dhaka, Hua Jiang, Anton Autere, Harri Lipsanen, Zhipei Sun and Henri Jussila

Sci Adv **4** (7), eaar7954.
DOI: 10.1126/sciadv.aar7954